Feasibility analysis for air-breathing electric propulsion spacecraft

1st International Symposium
on Very Low Earth Orbit Missions and Technologies

M. Tisaev[(1)], E. Ferrato [(2)], V. Giannetti [(2)], C. Paissoni [(2)], N. Baresi[(1)], A. Lucca Fabris[(1)], T. Andreussi [(2)]

[(1)] Surrey Space Centre, University of Surrey, Guildford, GU2 7XH, UK, email: m.tisaev@surrey.ac.uk
[(2)] SITAEL S.p.A., Via A. Gherardesca 5, 56121 Pisa, Italy

Abstract: Air-breathing electric propulsion (ABEP) enables long lifetime missions at very low orbital altitudes through the use of drag compensation. A model of the spacecraft is developed based on the interaction between thruster, intake and solar arrays. A quadratic solution is found in terms of specific impulse and evaluated at varying altitudes to identify the thruster performance required for drag-compensation. An upper altitude limit around 193km is based on a minimum thruster propellant density, resulting in approximate required values of I_{sp} > 3200s and T/P > 7mN/kW for a realistic ABEP spacecraft. Simulations of the ABEP spacecraft orbit with time reveal an unavoidable orbit eccentricity due to non-spherical gravity and therefore increased atmospheric variability. A thruster control law is introduced which avoids a divergent altitude behaviour by preventing thruster firings around the orbit periapsis. Through the combination of an initial frozen orbit, thruster control and an augmented T/P, a stable long-term profile is demonstrated based on the performance data of a gridded-ion thruster tested with atmospheric propellants. An initial mean semi-major axis altitude of 200km, a spacecraft mass of 200kg, I_{sp} = 5450s and T/P = 20mN/kW results in an altitude range of around 10-15km at altitudes of around 160-180km relative to the mean Earth radius for a constant, average solar activity.

I. Introduction

Electric propulsion for spacecraft offers a high specific impulse, low-thrust profile that is ideal for drag compensation in very low Earth orbit (VLEO). However, a conventional xenon-based system is limited in mission duration by the use of on-board propellant. The air-breathing electric propulsion (ABEP) concept uses gases in the upper atmosphere as the propellant source for spacecraft in VLEO. The thrust produced by the propulsion system counteracts atmospheric drag, allowing the use of orbits with a lower altitude than previously possible and a significant extension of the mission lifetime. A long-duration satellite in VLEO is attractive for many applications, such as increased resolution or smaller required aperture size for Earth observation missions, the possibility for science missions to collect data on atmospheric properties and geophysical fields at altitudes for which little data exists, and reduced latency for telecommunications satellites connecting to ground-based users (Crisp, et al., 2020).

It is crucial to determine how the thruster performance relates to the altitude at which drag-compensation can occur in order to assess the feasibility of an air-breathing spacecraft. The work of (Fujita, 2004) presented initial estimates of the altitude range based on a lower altitude limit due to spacecraft heating and an upper limit due to insufficient propellant density. A formulation for the minimum exhaust velocity required at different altitudes was identified based on the need to counteract the drag of a passive intake. The performance of such an intake was also modelled using Direct Simulation Monte-Carlo (DSMC) simulations, for which empirical fits were created. (Di Cara, et al., 2007) concluded that an air-breathing system was worthwhile at altitudes below 250 km by considering the propellant mass needed for conventional electric thrusters to provide a given operational lifetime in a dawn-dusk Sun synchronous orbit (SSO). (Romano, Binder, Herdrich, Fasoulas, & Schonherr, 2015) presented a method for finding drag in free-molecular flow, however a constant value for the drag coefficient was used in finding the thrust required for the purposes of reducing uncertainty. Unlike the previously noted studies, (Singh, 2014) and (Andreussi, et al., 2019) presented a more complete analysis of the spacecraft drag including the effect of lateral surfaces, such as solar arrays, which are assumed to be aligned parallel to the onset airflow. The latest work of (Andreussi, et al., 2019) developed a system analysis to optimise the thrust-to-drag ratio of an air-breathing thruster.

This review of the ABEP literature reveals the importance of including the drag contribution of lateral spacecraft surfaces to the drag-compensation analysis, which has been neglected in the majority of previous studies. The review also highlights a focus in existing literature on the development and optimisation of particular thruster designs. This study therefore aims to relate generic performance metrics of the air-breathing thruster and normalised spacecraft parameters to a feasible operating altitude, allowing identification of the flight envelope for an ABEP spacecraft. The

orbital variation with time of such an air-breathing spacecraft is subsequently investigated to determine the feasibility of a long-term, stable altitude profile. This differs from the majority of existing literature, in which a circular orbit is assumed, which is not naturally possible in the VLEO environment due to the non-sphericity of the Earth's gravity.

II. Dynamics and spacecraft parameters

The implemented system-level approach models the atmospheric properties, drag produced by different satellite surfaces and performance of a passive intake feeding air to the electric thruster. The model links the main components of the satellite platform by connecting the requirements of the air intake, electric propulsion system and solar arrays.

A. Spacecraft overview

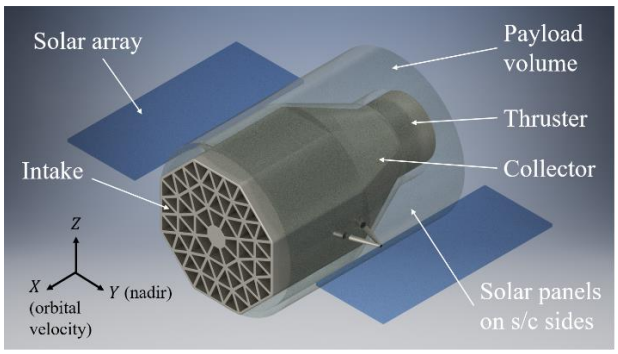

Figure II-1: Simplified spacecraft model.

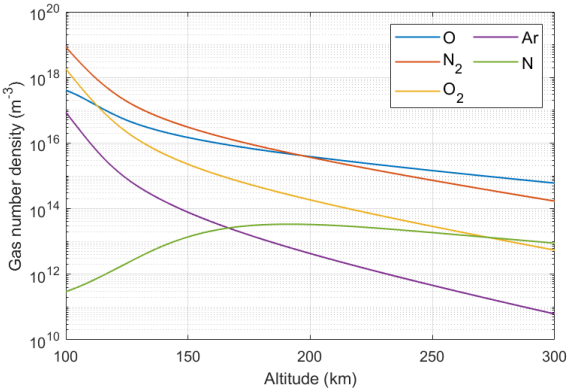

Figure II-2: Gas number density with altitude for average solar activity. Data is averaged over SSO latitudes/longitudes, times of day and days of year.

The ABEP principle is summarised in reference to the generic model shown in Figure II-1. The onset airflow passes through the intake and collector to the thruster. The air is decelerated before the entrance to the thruster to achieve compression to a higher density, and is then ionised and accelerated to produce thrust. The solar arrays are assumed to produce electrical power for the thruster, with both intake and solar array area needing to increase for a propulsion system producing a higher thrust. The nominal orientation of the satellite is assumed to be with the intake perpendicular to the onset flow and the solar arrays parallel to the flow vector. The orientation of the intake would be maintained perpendicular to the onset flow to maximise intake performance. A parallel solar array orientation to the flow is the preferred design for minimum drag. It is a realistic configuration for a SSO with a dawn-dusk terminator as it positions the array surface normal to the Sun vector for optimal power, as was the case for the ESA GOCE spacecraft (Drinkwater, Floberghagen, Haagmans, Muzi, & Popescu, 2003). The solar panel area A_P required is related to the thruster performance via the thruster electrical efficiency η_t:

$$A_P = \frac{F_T I_{sp} g_0}{2\eta_t a_P} \zeta \qquad \textbf{Equation 1}$$

where F_T is the thrust, I_{sp} the thruster specific impulse, g_0 the sea-level gravity acceleration, a_P the specific power per panel area and ζ the power margin to account for sub-systems other than the thruster. A nominal value of $a_P = 368 W/m^2$ is considered (a total panel efficiency of ~0.27) together with a margin ζ of 1.2. The panel area is assumed to be split between the array area A_a and panels mounted on the entire area of the spacecraft sides A_s, with a correction applied to account for the non-perpendicular orientation of A_s to the Sun vector. The dimensions of the cylindrical body are normalized using the spacecraft aspect ratio AR_s, which represents the ratio of body length to the intake diameter.

B. Atmospheric properties

The NRLMSISE-00 model is used to find the variation of atmospheric properties with altitude, providing data on air temperature T_∞, total density ρ_∞ and number density n of the air's constituent gases. (Picone, Hedin, Drob, & Aikin, 2002). The effect of altitude on gas number density and composition is shown in Figure II-2. The model includes the effect of solar activity on atmospheric properties, in the form of an input for the 10.7cm solar radio flux index $F10.7$ and the magnetic Ap index. In line with literature (Romano, et al., 2018), values of $F10.7 = 140, Ap = 15$ are assumed for average solar activity. The atmospheric properties vary appreciably with solar activity, geographic location and time of year. At a reference altitude of 180km where O and N_2 are the dominant species, a variability in total onset number density of 0.8-2.7×10^{16}m^{-3} and in O fraction of 0.1-0.6 can be expected for a mission lifetime of the same order as an 11-year solar cycle. Set atmospheric properties are assumed at each altitude for the drag-compensation analysis, which are obtained by averaging over times of day, days of year and a vector of latitudes/longitudes representative of an SSO. However, even for a constant altitude, the true atmospheric variability over the course of a single orbit as well as seasonal timescales supports the need for a time-propagated analysis. The drag-compensation analysis also assumes a circular orbit for the ABEP spacecraft, given that the solution is evaluated at each altitude. A set onset flow velocity u_∞ is found, which is equal to the orbital velocity at each altitude as per the Vis-Viva equation. While useful for an initial feasibility assessment, this circular orbit limitation is removed in the time-propagated analysis.

C. Drag calculations

The Knudsen number Kn is used to identify that the airflow in the VLEO altitudes of interest is in the free-molecular regime. This is based on a requirement of $Kn > 10$, which is found to occur at an altitude of around 132km. In the free-molecular flow regime, the air is assumed to act as individual particles and forces imparted on the body are calculated from the momentum transfer of particle collisions. Based on the process of (Schaaf & Chambre, 1958) and (Bird, 1994), the pressure and shear stresses are calculated from the difference between incident and reflected momentum flux of particles, and integrated to give a drag coefficient. The nature of particle collisions with the surface is simplified as either diffuse or specular. The average proportion of diffuse reflections is σ and the fraction of specular reflections simply $\epsilon = 1 - \sigma$. The molecular speed ratio S_∞ is defined below, which is equivalent to the Mach number in continuous flow:

$$S_\infty = \frac{u_\infty}{\sqrt{2RT_\infty}} \qquad \textbf{Equation 2}$$

where R is the specific gas constant. The analytical formulation for the drag coefficient C_D of a flat plate in molecular flow includes terms from both specular and diffuse reflections, and therefore depends on the angle α of the flat plate to the onset flow (Bird, 1994):

$$\begin{aligned} C_D = {} & \frac{B[1 - \epsilon\cos(2\alpha)]}{\sqrt{\pi}S_\infty} e^{-S_\infty^2 \sin^2(\alpha)} \\ & + \frac{\sin(\alpha)}{S_\infty^2}[1 + 2S_\infty^2 + \epsilon(1 - 2S_\infty^2\cos(2\alpha))]\,\mathrm{erf}(S_\infty \sin(\alpha)) \\ & + \frac{(1-\epsilon)}{S_\infty}\sqrt{\pi}\sin^2(\alpha)\sqrt{\frac{T_r}{T_\infty}} \end{aligned} \qquad \textbf{Equation 3}$$

where erf is the error function and T_r is the temperature of the reflected particles (assumed equal to the wall temperature T_w). To account for all major spacecraft surfaces, a drag coefficient value is found for each of the intake ($C_{D,i}$), arrays ($C_{D,a}$) and spacecraft side surfaces ($C_{D,s}$). Assuming an effective attitude control system, the intake is modelled as perpendicular to the flow ($\alpha = 90°$) and the arrays and spacecraft sides are parallel ($\alpha = 0°$). The first term on the right-hand side corresponds to the skin-friction drag and so B represents the number of surface sides exposed to the onset flow, resulting in $B = 2$ for the arrays and $B = 1$ otherwise. The value of σ has a large influence on the drag coefficient, particularly as skin-friction drag only occurs as a result of diffuse reflections. It is commonly

assumed that reflections are almost fully diffuse ($\sigma \to 1$) in orbital conditions (Schaaf & Chambre, 1958), so $\sigma = 0.9$ is used here.

D. Intake performance

This study assumes a passive intake which forms the full frontal area of the spacecraft, as this concept is considered the most widely-applicable due to its simplicity. The aspect ratio of the intake duct AR_i compares the intake length to the diameter. As indicated in Figure II-1, the division of the frontal area into smaller diameter sections results in a larger effective AR_i. The first function of the intake is to collect the mass flow of incoming air into the thruster, for ionisation and acceleration. This is represented by the collection efficiency η_c, which is the ratio between the thruster mass flow rate at the intake exit $\dot{m}_t$ and the onset flow rate $\dot{m}_\infty = \eta_c \rho_\infty A_i u_\infty$ (where A_i is the intake area). The second principal function is to increase the density of air by compressing the onset n_∞ to a higher value at the thruster n_t. A sufficiently high density is required to create plasma properties inside the thruster that allow propellant acceleration. This is represented by the compression ratio β, which is the density ratio between the intake entrance and exit. A compromise exists for a passive intake design between η_c and β due to the inverse relationship between flow velocity (and so a large $\dot{m}_t$) and the residency time of particles in the collector (and so a large n_t).

An η_c range of 0.3-0.5 is used here as this is the typical range predicted by previous studies (Fujita, 2004) (Romano, Binder, Herdrich, Fasoulas, & Schonherr, 2015). The maximum possible stagnation compression ratio is derived from isentropic flow theory. A more realistic value of β originates from the interpolation method developed by (Fujita, 2004), which accounts for the effect of T_w, AR_i and η_c as a correction factor to the stagnation compression ratio. For a representative $\eta_c = 0.35$ and $AR_i = 14$, this results in $\beta \approx 100$ at altitudes between 150 and 250km.

III. Drag-compensation analysis

A 1D steady-state equation of motion along the orbital direction is derived for the air-breathing spacecraft using force equilibrium, i.e. thrust F_T = total drag F_D. This results in a quadratic equation in terms of I_{sp}, which reveals that drag compensation is purely dependent on the efficiencies of the intake, solar panels and thruster, rather than the absolute thrust value. The simulation input parameters used to obtain the results presented in the following sections are shown in Table III-1, unless otherwise noted.

Table III-1: Input variables for simulations.

Intake	η_c	0.35
	AR_i	14
Power	η_t	0.5
	a_P	368 W/m^2
	ζ	1.2
Solar activity	$F10.7$	140
	Ap	15
Spacecraft	AR_s	3
Thruster	$\boldsymbol{n_{t,lim}}$	10^{18} m^{-3}

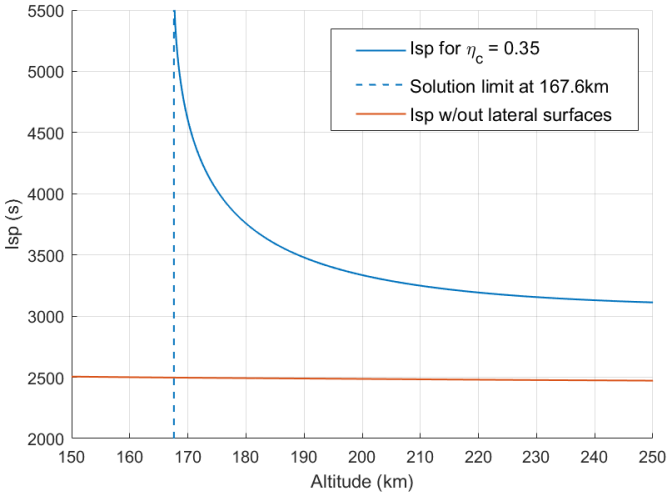

Figure III-1: I_{sp} solutions with altitude.

The behaviour of the I_{sp} solution with altitude is shown as the blue curve in Figure III-1, where it is compared to the solution if neglecting the drag from solar arrays and spacecraft sides (orange curve). The full solution tends to the orange curve at higher altitudes since less thrust is required, meaning solar array area diminishes, and the constant

offset is purely from spacecraft side drag. However, at lower altitudes there is a significant drag component from the solar arrays needed to power the thruster and the I_{sp} must increase in order to avoid generating less thrust than drag, before reaching an asymptotic limit. A real solution does not exist below a certain altitude, which is shown by the vertical dashed line and occurs at around 168km for these simulation parameters. This result indicates that the realistic power required by the thruster is a significant factor in defining the lower altitude limit of an air-breathing spacecraft. By evaluating β at each altitude and defining a minimum thruster propellant density, such as a typical value of $n_{t,lim}$ = 10^{18} m^{-3} (Fujita, 2004), an upper altitude limit is identified at which point the onset flow density is insufficient for thruster operation.

The operating altitude can be expressed as a function of the generic thruster performance figures: I_{sp} and T/P, which represent the propellant and power usage of the thruster respectively. The altitude corresponding to $n_{t,lim}$ = 10^{18} m^{-3} is evaluated in this case as 193.2km. Since an ABEP spacecraft needs to operate at altitudes below this value, the envelope of required thruster performance can be identified. For these spacecraft, intake and simulation parameters, a minimum I_{sp} of around 3200s and minimum T/P of around 7mN/kW are required. A reduced performance level can be tolerated if $n_{t,lim}$ is lowered, such that feasible drag-compensation could occur at higher altitudes.

IV. Orbit propagation of an ABEP spacecraft

The drag-compensation analysis serves as a useful first order design tool to assess the feasible altitude for a given level of generic thruster performance. However, the propagation of the spacecraft orbit with time is informative in observing the coupled nature of spacecraft thrust, altitude and properties of the onset airflow. Data for existing thrusters operated with atmospheric gases as propellant is used as a stringent method of simulating thruster performance for the simulations. The results of (Cifali, et al., 2011) and (Lotz, Collingwood, & Feili, 2012) are used here, in which the RIT-10-EBBM prototype was tested with varying mixtures of oxygen and nitrogen. The tests were conducted at fixed thrust levels using a range of propellant flow rates, resulting in varying thruster power. Operation of the thruster at F_T = 7.16mN and power of 560W with $\dot{m}_t$ = 6sccm of a $0.56N_2$ + $0.44O_2$ mixture, designed to replicate the gas element composition at a 200km VLEO altitude, resulted in a nominal operating point of I_{sp} = 5455s and T/P = 12.8mN/kW. This performance of the RIT-10-EBBM is promising for the development of an ABEP system, especially given that the thruster design is optimized for xenon, as the drag-compensation analysis predicts that operation is possible at an altitude of around 180km.

For the orbit propagations, a constant F_T = 7.16mN is only available when $\dot{m}_t$ > 0.13mg/s (equivalent to the minimum 6sccm tested by (Lotz, Collingwood, & Feili, 2012)). For larger onset flow rate values, $\dot{m}_t$ is limited to the maximum tested 15sccm or 0.36mg/s. The normalized formulation of drag-compensation analysis allows the required intake area to be defined for a given thruster power, in this case the maximum tested 560W. A_i = $0.1m^2$ is therefore used, which results in an array area of $1.64m^2$. Since the propellant density during tests is not reported, an acceptable n_t range of 10^{18}-$10^{19}m^{-3}$ is assumed, outside of which the thruster is modelled as inactive.

The orbital profile of the air-breathing spacecraft is simulated using a high-accuracy orbit propagator with variable-timestep integration, which accounts for high-order harmonics of the Earth's gravity and evaluates the NRLMSISE-00 atmospheric model at each timestep. Due to the extremely low orbital altitude, the non-sphericity of Earth's gravity has a significant effect on the satellite's motion and results in unavoidable eccentricity of the orbit. This is significant given that even a small change in altitude of several 10's km can require a considerably different level of thruster performance.

It is desirable to avoid large variations in atmospheric properties because of a large orbit eccentricity, as this will result in the thruster spending significant parts of the orbit outside of the operating range for $\dot{m}_t$ and n_t. A frozen orbit is therefore used to initialise the thruster in an orbit with reduced eccentricity and one which is stable over the long-term, at least when negating the effects of thrust and drag. This can be done with an analytical method when accounting for the J_2 and J_3 zonal gravity harmonics, for which the process of (Rosengren, 1989) is followed here and combined with a condition on the time derivative of the Right Ascension of the Ascending Node to also ensure a dawn-dusk SSO. The resulting mean orbital element set is transformed to osculating elements using the long version of the Brouwer-Lyddane theory (Brouwer, 1959) (Lyddane, 1963), which considers both short and long period motion of the orbit with zonal harmonics from J_2 to J_5.

A spacecraft mass of 200kg is used for the propagations that follow as a representative value for the spacecraft size and the orbit is initialised at a mean semi-major axis altitude $\bar{a}_0$ of 200km. The initial altitude profile without thrust is shown in Figure IV-1, which displays the orbital altitude relative to the mean Earth radius (orbit magnitude $|r| - R_E$)

and the true height above the geodetic surface. The eccentricity due to non-spherical gravity is indicated by the immediate $|r| - R_E$ periapsis-apoapsis range of 30km. Re-entry is shown to occur after 15 days in this case.

The inclusion of the thruster acts to extend the time on orbit, with the as-tested RIT-10-EBBM performance extending the re-entry time to 59 days. While this demonstrates the effectiveness of the thruster, the performance is not sufficient to raise $\bar{a}$ at any point in the profile. An increase in thruster T/P is therefore introduced, which has the effect of reducing the array area (and so array drag) while keeping the remaining thruster parameters unchanged. The aim of this approach is to investigate how much of an increase in performance is required to sustain a stable altitude profile. An increase to T/P = 20mN/kW successful in raising $\bar{a}$ over time and so further extends the profile up to a re-entry time of 88 days. However, a divergent altitude behaviour is identified after approximately 60 days. The effect of the thruster is clearly visible at this time by the increasing orbit apoapsis, however there is a simultaneous decay in periapsis which is not corrected by the thruster firings. This behaviour occurs because the thruster only activates around the periapsis of the orbit, when $\dot{m}_t$ and n_t are above the minimum level. Since an applied thrust affects the orbit radius at a point 180° from the current location, this thruster behaviour lifts the apoapsis, while the periapsis continues to fall since the thruster does not function in the higher regions of its orbit.

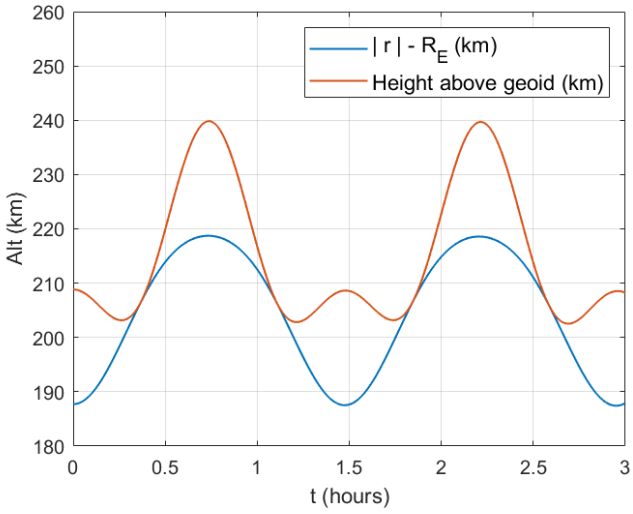

Figure IV-1: Initial propagated altitude profile without thrust (m=200kg, $\bar{a}_0$=200km, A_i=0.1m², T/P=12.8mN/kW).

A thruster control law is used to avoid the divergent altitude behaviour. The design approach for this control law is to prevent the thruster from firing around the periapsis of the orbit, which is based on an evaluation of mean orbital elements at each thruster timestep. For instance, the thruster is prevented from firing when the spacecraft position is within 10% of the current mean orbit periapsis, as a ratio of the instantaneous periapsis to apoapsis range. The use of the thruster control law is effective in avoiding the divergent altitude behaviour and achieves a stable, long-term altitude range, simulated over a two-year period. The controller achieves a minimised altitude range of 10-15km, with an altitude profile that translates to a height above the geodetic Earth surface of between 161km and 201km. This true height above the sub-spacecraft topology is the key value in determining the atmospheric properties. The range therefore corresponds well to the approximate value of 180km predicted by the drag compensation analysis. After an initial descent from $\bar{a}_0$ = 200km and subsequent settling period, the long-term variation of the altitude closely follows the seasonal variation in average n_∞, which changes the altitude at which the acceptable thruster density range occurs. For a 200kg spacecraft, an increase from 12.8mN/kW up to 20mN/kW is required given realistic variability of the atmospheric properties assuming average and constant solar activity. It is expected that such a T/P increase is required above the results given by the drag-compensation analysis since there are significant periods of a realistic, eccentric orbit where the thruster cannot fire due to air density and mass flow limitations, and this period is only increased with thruster control.

V. Conclusions

The drag-compensation analysis highlights the importance of drag from surfaces aligned parallel to the flow, such as the arrays and spacecraft sides. A solution for specific impulse with altitude is derived, using atmospheric properties that are averaged at each altitude, and is combined with an upper altitude limit based on a minimum required thruster air density to identify the thruster performance envelope. For realistic spacecraft properties, a minimum I_{sp} = 3200s and T/P = 7mN/kW are required for operation below the upper altitude limit of 193km.

The propagation of an air-breathing spacecraft's profile with time highlights the unavoidable orbit eccentricity introduced due to the non-spherical gravity in VLEO, resulting in variable altitude and flow properties over the orbit. The performance data of the RIT-10-EBBM thruster tested with an N_2 + O_2 mixture is used for the altitude propagations as a robust method of assessing the feasibility of an air-breathing spacecraft. The thruster nominal

operating point is I_{sp} = 5450s and T/P = 12.8mN/kW at 560W, with limits imposed for mass flow rate and propellant density. The orbital simulations show a divergent altitude behaviour which results in re-entry, and this is addressed with a thruster control law that prevents thruster firing around the orbit periapsis. A combination of an initial frozen orbit, the thruster control law and an increased T/P above the tested value is successful in establishing a stable, long-term operating altitude. A spacecraft mass of 200kg, initial mean semi-major axis of 200km, thruster control within 10% of the periapsis (as a ratio of the periapsis-apoapsis range) and T/P = 20mN/kW results in an altitude range of around 10km, which occurs at altitudes of approximately 160-180km relative to the mean Earth radius. This simulation of an existing Xe-designed thruster bodes well for the development of an ABEP system as part of the AETHER project, which aims to tailor the thruster design to the VLEO environment.

VI. Acknowledgements

This work has been partly performed within the AETHER project, funded by the European Union's Horizon 2020 research and innovation programme under grant agreement No 870436. This reflects only the author's view and the European Commission is not responsible for any use that may be made of the information it contains. M. Tisaev thanks the Doctoral College of the University of Surrey for his PhD scholarship.

VII.References

Andreussi, T., Ferrato, E., Giannetti, V., Piragino, A., Paissoni, C., Cifali, G., & Andrenucci, M. (2019). Development Status and Way Forward of SITAEL's Air-breathing Electric Propulsion Engine. *AIAA Propulsion and Energy 2019 Forum.* Indianapolis, USA. Retrieved from https://arc.aiaa.org/doi/abs/10.2514/6.2019-3995

Bird, G. (1994). *Molecular Gas Dynamics and the Direct Simulation of Gas Flows* (2nd ed.). Clarendon Press.

Brouwer, D. (1959). Solution of the problem of artificial satellite theory without drag. *The Astronomical Journal, 64*, 378. doi:10.1086/107958

Cifali, G., Misuri, T., Rossetti, P., Andrenucci, M., Valentian, D., Feili, D., & Lotz, B. (2011). Experimental characterization of HET and RIT with atmospheric propellants. *32nd International Electric Propulsion Conference.* Wiesbaden, Germany. Retrieved from http://electricrocket.org/IEPC/IEPC-2011-224.pdf

Crisp, N., Roberts, P., Livadiotti, S., Oiko, V., Edmondson, S., Haigh, S., . . . Schwalber, A. (2020). The benefits of very low earth orbit for earth observation missions. *Progress in Aerospace Sciences, 117*, 100619. Retrieved from https://doi.org/10.1016/j.paerosci.2020.100619

Di Cara, D., Amo, J. G., Santovincenzo, A., Dominguez, B. C., Arcioni, M., Caldwell, A., & Roma, I. (2007). RAM Electric Propulsion for Low Earth Orbit Operation: an ESA study. *30th International Electric Propulsion Conference.* Florence, Italy. Retrieved from http://electricrocket.org/IEPC/IEPC-2007-162.pdf

Drinkwater, M., Floberghagen, R., Haagmans, R., Muzi, D., & Popescu, A. (2003). GOCE: ESA's First Earth Explorer Core Mission. *Earth Gravity Field from Space - From Sensors to Earth Sciences*, (pp. 419-432). Bern, Switzerland. Retrieved from https://doi.org/10.1007/978-94-017-1333-7_36

Fujita, K. (2004). Air intake performance estimation of air-breathing ion engines. *Transactions of the Japan Soc. of Mech. Engineers, 70*(700), 3038–3044. Retrieved from https://www.jstage.jst.go.jp/article/kikaib1979/70/700/70_700_3038/_article

Lotz, B., Collingwood, C., & Feili, D. (2012). Radio Frequency Ion Thrusters Operated with Non-Conventional Propellants. *Trudy MAI, 60*. Retrieved from http://trudymai.ru/eng/published.php?ID=35404&eng=Y

Lyddane, R. (1963). Small eccentricities or inclinations in the Brouwer theory of the artificial satellite. *The Astronomical Journal, 68*, 555. doi:10.1086/109179

Picone, J., Hedin, A., Drob, D., & Aikin, A. (2002). NRLMSISE-00 empirical model of the atmosphere: Statistical comparisons and scientific issues. *Journal of Geophysical Research: Space Physics, 107*(A12), 1468. Retrieved from https://doi.org/10.1029/2002JA009430

Romano, F., Binder, T., Herdrich, G., Fasoulas, S., & Schonherr, T. (2015). Air-Intake Design Investigation for an Air-Breathing Electric Propulsion System. *34th International Electric Propulsion Conference.* Hyogo-Kobe, Japan. Retrieved from https://electricrocket.org/IEPC/IEPC-2015-269_ISTS-2015-b-269.pdf

Romano, F., Massuti-Ballester, B., Binder, T., Herdrich, G., Fasoulas, S., & Schönherr, T. (2018). System analysis and test-bed for an atmosphere-breathing electric propulsion system using an inductive plasma thruster. *Acta Astronautica, 147*, 114-126. Retrieved from https://doi.org/10.1016/j.actaastro.2018.03.031.

Rosengren, M. (1989). Improved technique for passive eccentricity control. *Orbital Mechanics and Mission Design; Proceedings of the AAS/NASA International Symposium*, (pp. 49-58). San Diego, USA.

Schaaf, S., & Chambre, P. (1958). *Flow of rarefied gases.* Princeton University Press.

Singh, L. (2014). *Very low earth orbit propellant collection feasibility assessment.* PhD thesis, Georgia Institute of Technology, Aerospace Eng.